Efficient coupling to strongly confined nanowire plasmons

E. Verhagen*, M. Spasenović, A. Polman, and L. Kuipers

FOM Institute for Atomic and Molecular Physics (AMOLF),

Kruislaan 407, 1098 SJ Amsterdam, The Netherlands

*e-mail: verhagen@amolf.nl

The ability to guide and store optical energy on subwavelength scales with surface plasmon polaritons (SPPs) offers a wealth of opportunities for exciting science and applications. Their potential includes efficient sensing[1], the enhancement of nonlinear effects[2-4], the miniaturization of optical interconnects[5-7] and strong interactions with individual quantum emitters[8,9]. While various strategies for guiding SPPs such as nanoparticle chains[10,11], nanowires[12-15] and channel- and slot waveguides[5,6] have been explored, excitation of highly confined modes remains difficult. Here we experimentally demonstrate the efficient excitation of nanowire SPP modes at telecom frequencies through adiabatic transformation of a macroscopic wave. The SPPs propagate for substantial lengths along nanowires with diameters as small as 60 nm. Phase-sensitive near-field investigation reveals the nature of the mode and explains the excitation mechanism. Two adiabatic tapers and a nanowire are combined in an input-output device, of which the high efficiency opens avenues for truly subwavelength photonic circuitry.

A metallic cylinder guides radially polarized electromagnetic waves for all frequencies smaller than the surface plasmon resonance frequency. At THz frequencies and below, these so-called Sommerfeld waves are weakly guided[16,17]. In the optical and near-infrared regime however, the analogous SPP wave propagating along a metal nanowire is predicted to become strongly confined to the nanowire when its radius is reduced to tens of nanometers[12,18,19]. From here on this mode will be called 'the nanowire mode'. Nanowires truncated to finite lengths act

as optical nanoantennas for the efficient harvesting or emission of light[19- 23]. However, the antenna design precludes further processing of optical information. To allow planar integration a mechanism is needed to efficiently transfer optical energy back and forth between the nanoconfined wire SPP and a low-loss guided wave. A metallic stripe of μm-scale width is well known to guide SPPs[24,25]. By tapering it down to the desired nanowire size, we obtain the required coupling element. Along the taper the proper SPP mode is adiabatically transformed to the nanowire mode[18].

Figure 1 explains the transformation mechanism. It presents the calculated width dependence of the effective mode index $n_{eff} = \mathrm{Re}\{k_{\|}\}/k_0$ of the fundamental mode guided by a 77 nm thick straight Au stripe on glass for various wavelengths. When the width is reduced, the mode becomes more strongly confined and n_{eff} diverges. At small widths the mode is recognizable as the nanowire mode; it is highly confined around the nanowire and has approximately 'radial' polarization. The strong interaction of the optical field with surface charges on the metal leads to a pronounced longitudinal electric field component. For longer wavelengths, n_{eff} is first slightly reduced when the waveguide narrows, because the fraction of the modal field guided in air increases through the mode transformation. Importantly, for large widths the field is predominantly localized at the substrate side of the guide. This mode is responsible for the focusing of SPPs on the substrate side of a laterally tapered metal film[26]. Air-guided modes, which have previously been used to excite waveguides of subwavelength width[27,28], are unsuitable for adiabatic coupling to the nanowire mode (see supplementary material).

In the experiment (see Fig. 1(b)) the desired mode on the substrate side of a Au film on glass is excited at the entrance of a 5 μm wide waveguide with 1550 nm light using a hole array with a 1 μm pitch. The evanescent SPP field is probed above the sample with a phase-sensitive near-field microscope which yields both the local field amplitude $|A|$ and the phase φ[29]. The complex signal $A = |A|e^{i\varphi}$ is a projection of the vectorial near field on the polarization state in the

reference beam. An optical microscope image of the structure is shown in Fig. 2(a); Fig. 2(b) is an SEM micrograph of the coupling region. The width of the waveguide decreases over a length of 20 μm after which the waveguide connects to a nanowire.

Figure 2(c) shows a map of the measured amplitude $|A|$. In the left of the image, the hole array is visible with which the SPPs are excited. In the tapered section the presence of SPPs propagating at the Au/glass interface is only evidenced by a field amplitude along the edge of the waveguide. At the end of the taper, the SPPs couple to a 150 nm wide nanowire. Near the end of the taper a clear amplitude increase is observed as the guided wave becomes more strongly concentrated and the fraction of the modal field in air increases. The SPP wave is guided along the 40 μm long wire until the wire terminates in a continuous Au film. The full width at half maximum of the intensity in the guided beam is 300 nm, which constitutes only an upper limit to the mode size as the probe diameter was 220 nm. The transverse size of the guided mode is therefore considerably smaller than the 1550 nm free-space wavelength.

To investigate the nature of the excited nanowire mode, we measure the spatial profile of $|A|\cos(\varphi)$ while varying the polarization of the reference beam. Figures 3(a) and (b) show near-field images of the coupling region, containing the end of the taper and the start of the nanowire, obtained with orthogonal polarization angles labelled $\theta = 0°$ and $\theta = 90°$. The wave visible at the edges of the taper is gradually converted to a wave propagating along the nanowire. Whereas the phase fronts on the nanowire in Fig. 3(a) are quite symmetric with respect to the center of the wire, they are largely asymmetric in Fig. 3(b). Because of the symmetry of the experimental geometry, purely symmetric and antisymmetric images are expected for the proper polarizations of the reference branch. The symmetric and antisymmetric field maps can be retrieved from the measurements at $\theta = 0°$ and $\theta = 90°$ through a simple linear transformation (see supplementary material). Apart from a minor asymmetry, attributable to small measurement imperfections, we obtain highly symmetric and antisymmetric field maps, displayed in Figs. 3(c) and (d).

The observed symmetries are intimately related to the symmetry of the nanowire mode. The calculated electric field components of the mode are depicted in Figs. 3(e-g), for the contour that the near-field probe follows. The pattern observed in Fig. 3(c) closely resembles that of the calculated longitudinal field E_x. E_x therefore provides the dominant contribution to the symmetric image, rather than E_z. Its amplitude is comparable to that of the measured antisymmetric transverse component E_y (compare the amplitudes in Figs. 3(c) and (d)). The presence of such a significant longitudinal field demonstrates the strong deviation of the highly confined nanowire mode from a transverse wave. The antisymmetric image indicates that the E_y fields have an opposite sign at opposite sides of the nanowire, proving that the 'radially' polarized nanowire mode is excited. The same symmetry is visible at the edges of the taper leading up to the nanowire. This observation proves that the coupling mechanism is a gradual development of the mode on the broad tapered waveguide to the nanowire mode.

From the phase evolution along the complete length of the nanowire the SPP wave vector is accurately determined. Figure 4(a) shows measured dispersion curves for nanowire widths of 60, 85 and 150 nm, obtained by varying the excitation laser wavelength. As expected, the largest wave vector is observed for modes on the narrowest nanowire. The measured effective mode indices n_{eff} and propagation lengths ($L = \frac{1}{2}\,\mathrm{Im}\{k_{\|}\}^{-1}$, obtained from exponential fits to the near-field maps) are compared to theory for 1550 nm in Fig. 4(b). For the two smallest widths, excellent agreement is found between measurements and calculations, which contain no adjustable parameters. The origin of the deviation for the 150 nm wide waveguide is as yet unknown; it indicates that the leakage into the substrate (which occurs for $n_{eff} < n_{glass}$) is larger than calculated. The excellent agreement between the measured and calculated propagation lengths for small widths indicates that Ohmic dissipation is the dominant loss mechanism, since the calculations neglect scattering losses.

To demonstrate the efficiency of the adiabatic coupler, we fabricated an input-output device consisting of two tapers connected by a 2 μm long nanowire. Figure 5(a) shows the measured amplitude distribution in the device. SPPs incident from the left are converted from a waveguide width of 2 μm to a 90 nm wide nanowire. In the output taper on the right, the transmitted SPPs are converted back to a 2 μm width. With a Fourier analysis we select only waves that propagate from left to right (Fig. 5(b)).[30] By comparing the amplitudes at the edges of the taper at 4 μm distance to either side of the nanowire, we determine the total intensity transmission to be 20±6%. From the Fourier analysis a 2±1% backreflection loss is found. Correcting for the known propagation loss of the 2 μm long nanowire (Fig. 4(b)), the *combined* coupling and decoupling efficiency of both tapers is calculated to be $I_{in}e^{-l/L}/I_{out} = 24 \pm 7\%$, with l the nanowire length. This corresponds to a 3 dB insertion loss per coupler. The loss includes dissipation in the tapers, scattering to free-space radiation and leakage of the mode into the substrate when $n_{eff} < n_{glass}$. Many parameters can be identified to improve the efficiency: the use of Ag will reduce Ohmic damping, an optimal tapering profile will balance adiabaticity and taper length, and leakage radiation can be eliminated by increasing the refractive index of the substrate or reducing the film thickness.

In conclusion, we have shown the excitation of highly confined nanowire SPP modes through the principle of adiabatic mode transformation. This mechanism ensures efficient coupling and allows straightforward integration of nanowires on planar substrates. Phase-sensitive near-field microscopy identified the radially polarized nature of the excited mode, and showed that this mode gradually evolves from the fundamental SPP mode propagating at the substrate side of a metal stripe waveguide. These results demonstrate a practical implementation of the nanoscale miniaturization of light on a chip and provide the necessary tools to interface the macro world with individual nano-objects through plasmonic circuitry.

Methods

Mode calculations

The bound and leaky modes of infinitely long waveguides with rectangular cross sections have been obtained with the finite-element method solver COMSOL Multiphysics. The optical constants and metal thickness were directly obtained from ellipsometry. The spatial element size varied from 0.1 nm at the corners of the waveguide to 100 nm far from the guide. Perfectly matched layer (PML) simulation boundaries were located many micrometers from the guide. Due to a nonzero reflectivity of the PML boundaries at very shallow incident angles, the determination of the fundamental mode is not possible for a free-space wavelength of 1550 nm between 200 and 550 nm widths. In Fig. 1(a), a cubic spline interpolation in this range is indicated by a dotted line. Throughout the calculations, convergence of n_{eff} to 10^{-5} was maintained.

Sample fabrication

The sample consists of a 77±3 nm thick Au film on BK7 glass (n_{glass} = 1.50 at 1550 nm). A layered resist stack consisting of 350 nm photoresist (S1813), 20 nm Ge and 100 nm negative electron beam resist (Ma-N 2401) was used. The pattern formed in the top film by electron beam lithography was transferred to the layers underneath by reactive ion etching. An Au film was evaporated directly on the substrate, and the remaining photoresist was removed by liftoff. The waveguide widths were determined from SEM micrographs.

Phase-sensitive near-field microscopy

The excitation source is a continuous-wave tunable laser with a wavelength ranging from 1450 to 1570 nm (varied in 2 nm steps). The evanescent field above the sample is probed at a height of ~20 nm by an Al-coated tapered fiber probe with an aperture diameter of ~220 nm. The sample

and near-field probe are incorporated in one branch of a Mach-Zehnder interferometer. The light in the probe fiber interferes with a frequency-shifted reference beam. The time-dependent interference signal is detected and analyzed with a lock-in amplifier.

The polarization in the reference branch is controlled. A spatial distribution of the measured complex signal $A = |A|e^{i\varphi}$ for any desired polarization angle θ of the reference branch can be constructed by superimposing two images taken at orthogonal polarizations $\hat{u}$ and $\hat{v}$ in the detection fiber:

$$A(\theta) = A_u \cos(\theta - \theta_u) + e^{i\Delta\varphi} A_v \sin(\theta - \theta_v), \quad (1)$$

where $\Delta\varphi$ is a phase offset between image A_u and A_v, which is determined by comparing the image constructed with equation (1) to images measured at several polarization angles θ.

Acknowledgements

This work was made possible by the facilities of the Amsterdam nanoCenter. It is part of the research programme of the Stichting voor Fundamenteel Onderzoek der Materie (FOM), which is financially supported by the Nederlandse organisatie voor Wetenschappelijk Onderzoek (NWO). Support of the EC-funded project PhOREMOST (FP6/2003/IST/2-511616) is gratefully acknowledged. This work was partially supported by NANONED, a nanotechnology program of the Dutch Ministry of Economic Affairs, and by the Joint Solar Programme (JSP) of FOM, which is co-financed by gebied Chemische Wetenschappen of NWO and Stichting Shell Research. M.S. acknowledges the support of the European Community under the Marie Curie Scheme (contract number MEST-CT-2005-021000). The authors thank Matteo Burresi, Dries van Oosten and Tobias Kampfrath for useful discussions.

Correspondence and requests for materials should be addressed to L.K.

Author contributions

E.V. and M.S. fabricated the structures and carried out the experiments. A.P. and L.K. supervised the project. All authors contributed to the interpretation and the writing of the manuscript.

References

[1] Nie, S. and Emory, S. R. Probing single molecules and single nanoparticles by surface-enhanced Raman scattering. *Science* **275**, 1102-1106 (1997).

[2] Bouhelier, A., Beversluis, M., Hartschuh, A., and Novotny, L. Near-field second-harmonic generation induced by local field enhancement. *Phys. Rev. Lett.* **90**, 013903 (2003).

[3] van Nieuwstadt, J. A. H. *et al*. Strong modification of the nonlinear optical response of metallic subwavelength hole arrays. *Phys. Rev. Lett*. **97**, 146102 (2006).

[4] Kim, S. *et al.* High-harmonicity generation by resonant surface plasmon field enhancement. *Nature* **453**, 757-760 (2008).

[5] Bozhevolnyi, S. I., Volkov, V. S., Devaux, E., Laluet, J.-Y., and Ebbesen, T. W. Channel plasmon subwavelength waveguide components including interferometers and ring resonators. *Nature* **440**, 508-511 (2006).

[6] Dionne, J. A., Lezec, H. J., and Atwater, H. A. Highly confined photon transport in subwavelength metallic slot waveguides. *Nano Lett.* **6**, 1928-1932 (2006).

[7] Ebbesen, T. W., Genet, C., and Bozhevolnyi, S. I. Surface-plasmon circuitry. *Phys. Today* **61**, 44-50 (2008).

[8] Chang, D. E., Sørensen, A. S., Demler, E. A., and Lukin, M. D. A single-photon transistor using nanoscale surface plasmons, *Nature Physics* **3**, 807-812 (2007).

[9] Akimov, A. V. *et al*. Generation of single optical plasmons in metallic nanowires coupled to quantum dots. *Nature* **450**, 402-406 (2007).

[10] Quinten, M., Leitner, A., Krenn, J. R., Aussenegg, F. R. Electromagnetic energy transport via linear chains of silver nanoparticles. *Opt. Lett.* **23**, 1331-1333 (1998).

[11] Maier, S. A. *et al.* Local detection of electromagnetic energy transport below the diffraction limit in metal nanoparticle plasmon waveguides. *Nature Mater.* **2**, 229-232 (2003).

[12] Takahara, J., Yamagishi, S., Taki, H., Morimoto, A., and Kobayashi, T. Guiding of a one-dimensional optical beam with nanometer diameter. *Opt. Lett.* **22**, 475-477 (1997).

[13] Dickson, R. M. and Lyon, L. A. Unidirectional plasmon propagation in metallic nanowires. *J. Phys. Chem. B* **104**, 6095-6098 (2000).

[14] Ditlbacher, H. *et al.* Silver nanowires as surface plasmon resonators. *Phys. Rev. Lett.* **95**, 257403 (2005).

[15] Knight, M. W., Grady, N. K., Bardhan, R., Hao, F., Nordlander, P., and Halas, N. J. Nanoparticle-mediated coupling of light into a nanowire. *Nano Lett.* **7**, 2346-2350 (2007).

[16] Sommerfeld, A. Fortpflanzung elektrodynamischer Wellen an einem zylindrischen Leiter. *Ann. der Physik und Chemie* **67**, 233-290 (1899).

[17] Wang, K. and Mittleman, D. M. Metal wires for terahertz wave guiding. *Nature* **432**, 376-379 (2004).

[18] Stockman, M. I. Nanofocusing of optical energy in tapered plasmonic waveguides. *Phys. Rev. Lett*. **93**, 137404 (2004).

[19] Novotny, L. Effective wavelength scaling for optical antennas. *Phys. Rev. Lett.* **98**, 266802 (2007).

[20] Mühlschlegel, P., Eisler, H.-J., Martin, O. J., Hecht, B., and Pohl, D. W. Resonant optical antennas. *Science* **308**, 1607-1609 (2005).

[21] Cubukcu, E., Kort, E. A., Crozier, K. B., and Capasso, F. Plasmonic laser antenna. *Appl. Phys. Lett.* **89**, 093120 (2006).

[22] Tang, L. *et al.* Nanometre-scale germanium photodetector enhanced by a near-infrared dipole antenna. *Nature Photon.* **2**, 226-229 (2008).

[23] Taminiau, T. H., Stefani, F. D., Segerink, F. B., and van Hulst, N. F. Optical antennas direct single-molecule emission. *Nature Photon.* **2**, 234-237 (2008).

[24] Weeber, J.-C., *et al.* Near-field observation of surface plasmon polariton propagation on thin metal stripes. *Phys. Rev. B* **64**, 045411 (2001).

[25] Zia, R., Selker, M. D., and Brongersma, M. L., Leaky and bound modes of surface plasmon waveguides. *Phys. Rev. B* **71**, 165431 (2005).

[26] Verhagen, E., Polman, A., and Kuipers, L. Nanofocusing in laterally tapered plasmonic waveguides. *Opt. Express* **16**, 45-57 (2008).

[27] Krenn, J. R. *et al.* Non-diffraction-limited light transport by gold nanowires. *Europhys. Lett.* **60**, 663-669 (2002).

[28] Yin, L. *et al.* Subwavelength focusing and guiding of surface plasmons. *Nano Lett.* **5**, 1399-1402 (2007).

[29] Balistreri, M. L. M., Korterik, J. P., Kuipers, L., and van Hulst, N. F. Local observations of phase singularities in optical fields in waveguide structures. *Phys. Rev. Lett.* **85**, 294-297 (2000).

[30] Engelen, R. J. P. *et al.* Ultrafast evolution of photonic eigenstates in *k*-space. *Nature Phys.* **3**, 401-405 (2007).

Figure Legends

Figure 1. Nanowire mode excitation by adiabatic transformation. a) Effective mode index of the fundamental SPP mode guided by a Au waveguide on glass as a function of waveguide width. The dots between 200 and 550 nm widths for 1550 nm are a cubic spline interpolation (see methods). The insets show cross sections of the electric field amplitude of the fundamental mode for 60 nm and 5 μm widths at a free-space wavelength of 1550 nm. b) Schematic depiction of the experiment. SPPs are excited at the substrate side of a tapered Au waveguide by focusing a laser beam on a hole array, and are coupled into a nanowire. Their evanescent field is probed by an Al-coated tapered fiber probe that is scanned above the sample. The signal is mixed with a reference beam in a heterodyne interferometric setup and the resulting signal is led to a detector and lock-in amplifier.

Figure 2. Near-field imaging of SPP excitation and propagation on a nanowire. a) Optical microscope image of the investigated structure. b) SEM micrograph of the coupling region. c) Collected near-field SPP amplitude. SPPs excited on the Au/glass surface in the left of the image are converted in the 20 μm long tapering region to a mode guided along a 150 nm wide waveguide.

Figure 3. Phase- and polarization-selective investigation of the nanowire mode. a,b) Measured near-field signal $|A|\cos(\varphi)$ in the region of coupling to a 150 nm wide waveguide, for two orthogonal polarizations of the reference branch. c,d) Symmetric and antisymmetric near-field images in a 2 μm long section of the nanowire obtained as described in the text. The dotted lines indicate the position where the near-field probe makes a height step due to the presence of the

nanowire. They are therefore separated further than the actual nanowire width. e-g) Calculated field components E_x, E_y and E_z at a height of 20 nm above the sample.

Figure 4. Nanowire mode dispersion. a) Measured dispersion curves for three Au waveguide widths. The dashed line denotes the dispersion of light in the substrate. The error bars represent the experimental uncertainty. b) Measured mode index n_{eff} and propagation length as a function of waveguide width (symbols), compared to calculations (curves) for a free-space wavelength of 1550 nm.

Figure 5. Input-output device based on adiabatic transformation to the nanowire mode. a) Near-field amplitude at λ = 1550 nm in a 2 μm long nanowire connected by tapered waveguide sections for input and output coupling. SPPs are incident from the left. b) Near-field amplitude of only forward propagating waves derived from (a). The intensity transmission is 20±6%.

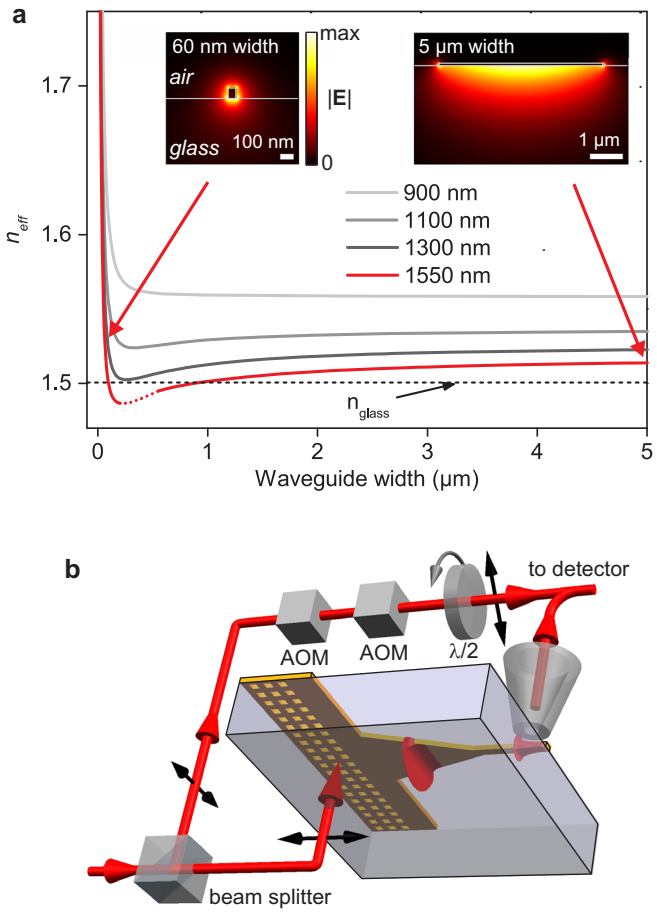
a
60 nm width
air
glass
100 nm
max
|E|
0
5 μm width
1 μm
900 nm
1100 nm
1300 nm
1550 nm
1.7
1.6
1.5
n_eff
n_glass
0
1
2
3
4
5
Waveguide width (μm)
b
to detector
AOM
AOM
λ/2
beam splitter

Figure 1

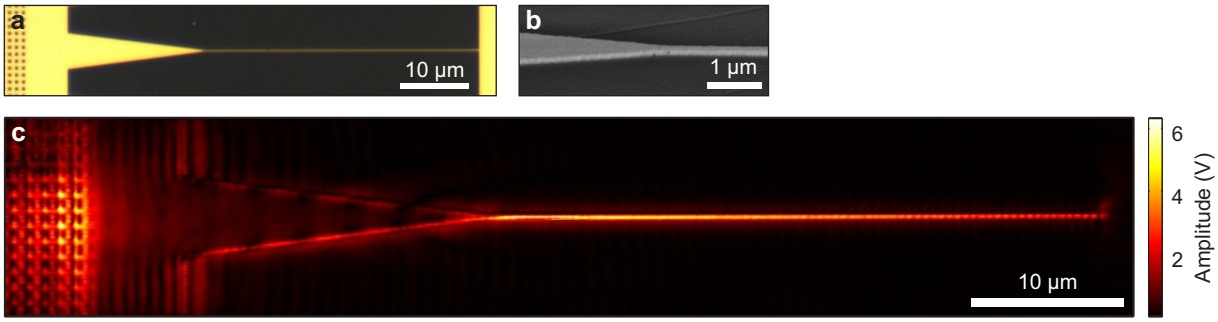

Figure 2

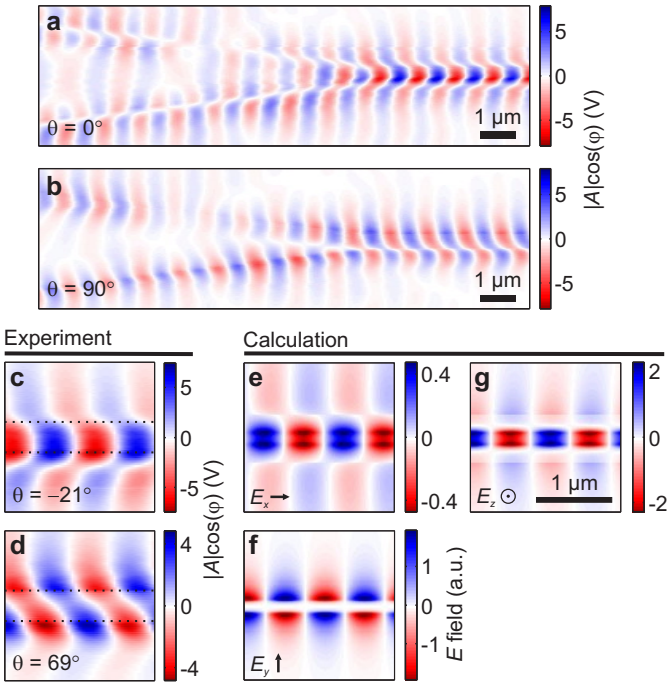
a
θ = 0°
1 μm
5
0
-5
b
θ = 90°
1 μm
5
0
-5
|A|cos(φ) (V)
Experiment
Calculation
c
θ = –21°
5
0
-5
d
θ = 69°
4
0
-4
|A|cos(φ) (V)
e
E_x
0.4
0
-0.4
f
E_y
1
0
-1
E field (a.u.)
g
E_z
1 μm
2
0
-2

Figure 3

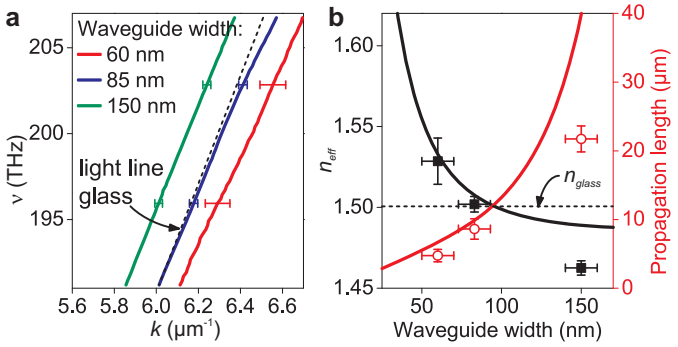
a
Waveguide width:
60 nm
85 nm
150 nm
light line
glass
205
200
195
ν (THz)
5.6 5.8 6.0 6.2 6.4 6.6
k (μm-1)
b
1.60
1.55
1.50
1.45
neff
nglass
40
30
20
10
0
Propagation length (μm)
50
100
150
Waveguide width (nm)

Figure 4

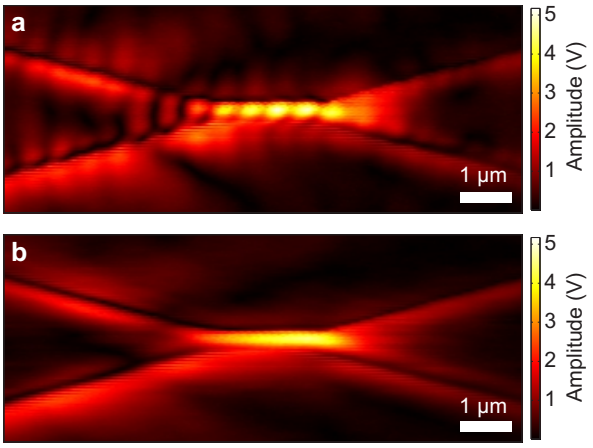

Figure 5